Shoshonitic liquid line of descent from diorite to granite: the Late Precambrian post-collisional Tismana pluton (South Carpathians, Romania)

Jean-Clair Duchesne [a,*], Tudor Berza [b], Jean-Paul Liégeois [c], Jacqueline Vander Auwera [a]

[a] *Laboratoires Associés de Géologie, Pétrologie et Géochimie, Université de Liège, B-4000 Sart Tilman, Belgium*
[b] *Institutul Geologic al României, Str. Caransebeş 1, Bucharest 78344, Romania*
[c] *Département de Géologie (Section de Géologie Isotopique), Musée Royal de l'Afrique Centrale, B-3080 Tervuren, Belgium*

Abstract

The post-collision late-kinematic Tismana pluton belongs to the shoshonitic series. It is part of a Late Precambrian basement within the Alpine Danubian nappes of the South Carpathians (Romania). This pluton displays an exceptionally complete range of compositions from ultramafic to felsic rocks (granites). Widespread mingling/mixing relationships at all scales give rise to a variety of facies. A liquid line of descent from the diorites to the granites is reconstructed by considering the variation in major and trace elements (REE, Sr, Rb, Ba, Nb, Zr, Hf, Zn, V, Co, Cr, U, Th, Ga, Pb) from 33 selected samples as well as mineral/melt equilibrium relationships. The first step of fractional crystallization is the separation from a monzodioritic parent magma of a peridotitic cumulate similar to the ultramafic rock found in the massif. A possible contamination by lower crustal mafic component takes place at this stage. The second step marks the appearance of apatite and Fe–Ti oxide minerals as liquidus phases, and the third step, saturation of zircon. Mixing by hybridisation of magmas produced at different stages of the evolution along the liquid line of descent is also operating (endo-hybridisation). As depicted by Nd and Sr isotopes, fractional crystallization was combined to an important early contamination by a mafic lower crust in a deep-seated magma chamber and to a later and mild contamination by a felsic medium crust in an intermediate chamber. The mingling essentially occurred during the final emplacement in the high-level magma chamber. The monzodioritic parent magma, identified by major and trace element modelling, is shown by Sr and Nd isotopes to have its source in the lithospheric mantle or in a juvenile mafic lower crust derived from it. The necessarily recent enrichment in K_2O and associated elements of the lithospheric mantle is likely to be related to the preceding Pan-African subduction period. The partial melting of this newly formed deep source has to be linked to a major change in the thermal state of the plate. © 1998 Elsevier Science B.V. All rights reserved.

Keywords: Post-collisional; Shoshonitic; Granitoids; Hybridisation; Pan-African; Romania

---

* Corresponding author. E-mail: jc.duchesne@ulg.ac.be

1. Introduction

The post-collisional period of an orogen probably encompasses the largest variability in chemistry, tectonic links and origin of magmatism in a single geodynamic setting. It is poorly understood, as it fits with difficulty in simplistic plate tectonic models. However, the tendency to produce high-K calc-alkaline and even alkaline granitoids after collision seems to be widespread (Bonin et al., 1987; Liégeois and Black, 1987; Sylvester, 1989). Extreme products such as the shoshonitic series (= very high-K calc-alkaline) are scarce but may throw a new light on post-collision events.

Such a shoshonitic series occurs in the Precambrian basement of Danubian Alpine nappes in the Romanian South Carpathians. The studied Tismana pluton encompasses a large and continuous range of compositions from ultramafic cumulates and diorites to granites. These different facies show remarkable mingling and mixing patterns that transform this granitoid pluton into a complex object. A requisite approach is therefore to first sort out the influence of mixing and fractional crystallization before reconstructing the genuine characteristics of the shoshonitic

source. We will show that Tismana gives evidence that a unique parental magma may produce a series of coexisting melts, which can in turn mix together to give rise to a series of hybrids (endo-hybridisation). In this process, interaction with medium and lower crustal rocks has been evidenced by isotopes at two stages of the fractionation process, but in too small amounts to be revealed by major and trace element modelling. Tismana thus points to complex multistage magma chamber processes and source composition within a post-collisional setting.

2. The South Carpathian Tismana pluton

Two tectonically juxtaposed Precambrian groups compose the basement of the Danubian nappes, the lowermost Alpine units in South Carpathians (Fig. 1). The first basement group, Dragşan, is mainly amphibolitic and represents a ca. 800 Ma old oceanic island arc (Liégeois et al., 1996), subsequently metamorphosed in an HP-HT amphibolite subfacies. The second basement group, Lainici-Păiuş, is metasedimentary, mainly quartzitic, older than 588 Ma (U–Pb
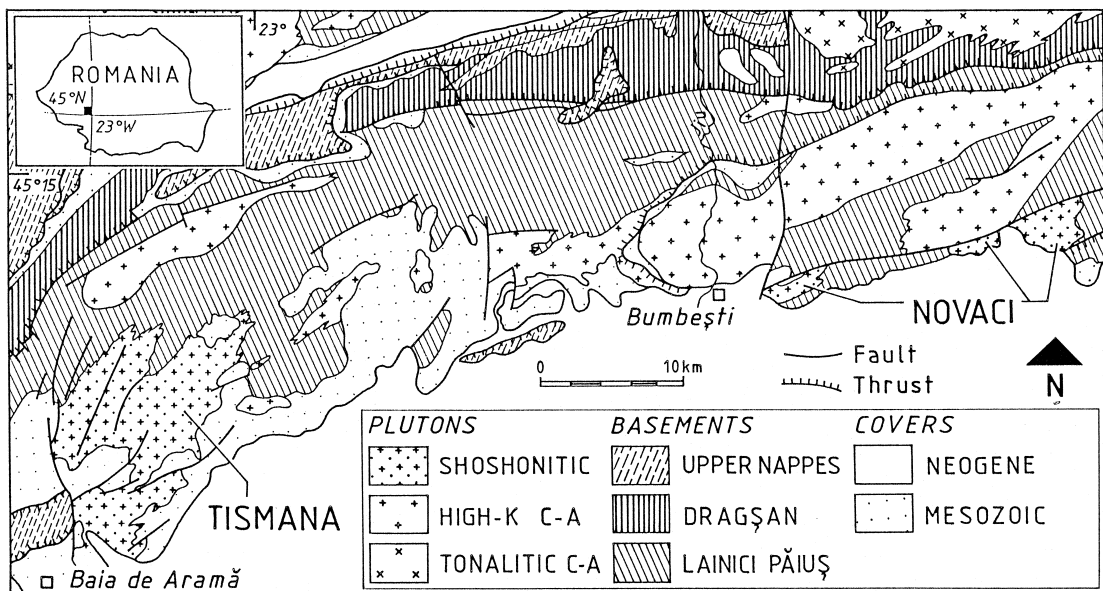

Fig. 1. Simplified geological map of the Danubian window in South Carpathians (from Liégeois et al., 1996) enhancing the Precambrian lithologies. C-A means calc-alkaline. The upper nappes group the Getic and the Upper Danubian nappes.
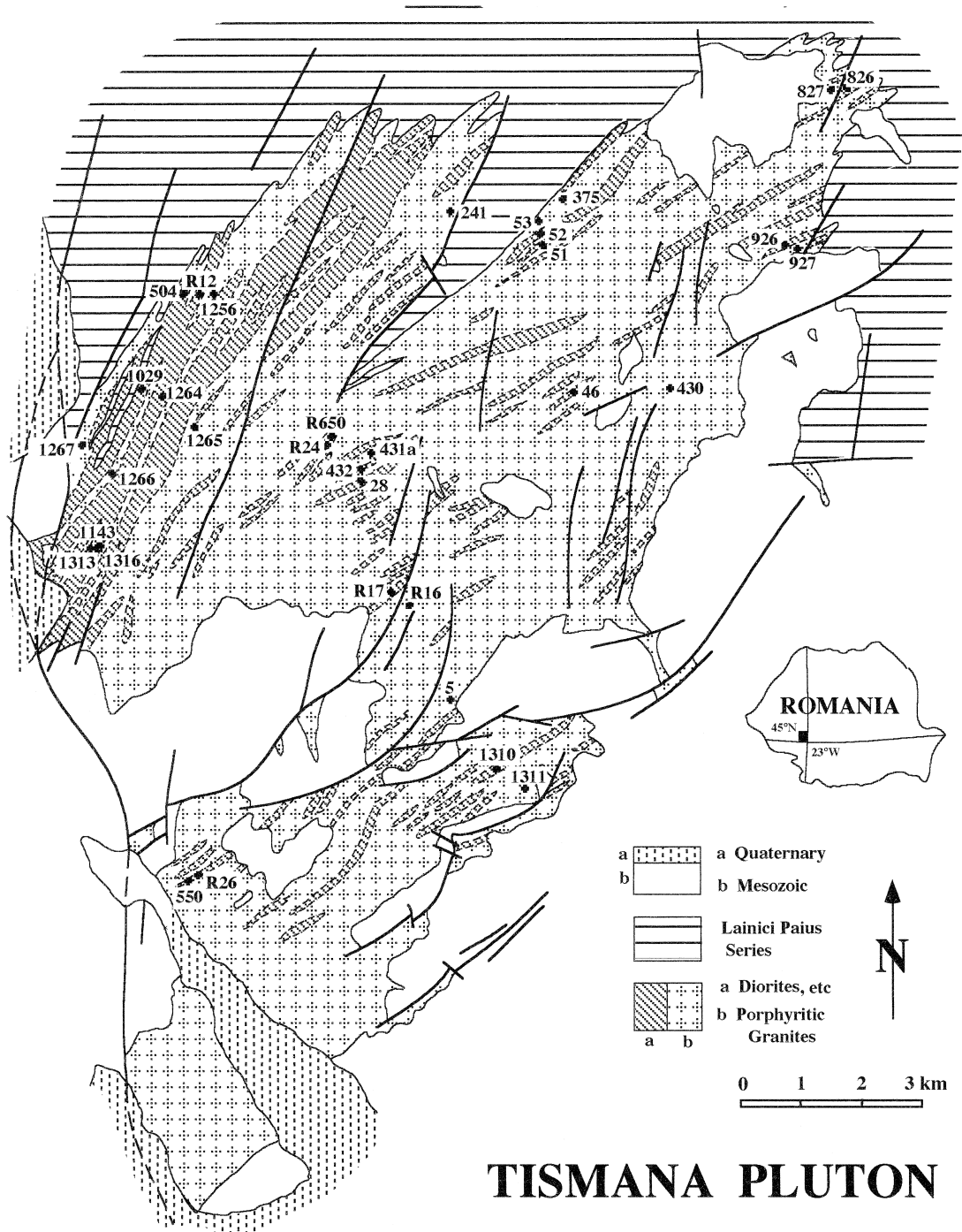
Fig. 2. Geological map of the Tismana pluton (after Berza, 1978). The smaller strips are not at scale, most of them being only a few metres thick; the larger strips of equigranular mafic rocks are interleaved with irregular porphyritic granites dykes or bands.

zircon; Grünenfelder et al., 1983), and has been metamorphosed in a LP-HT amphibolite subfacies. Both basement groups have been intensely intruded by granitoids, but only Lainici-Păiuş metasediments are cut by late-kinematic plutons with shoshonitic compositions, the Tismana and Novaci massifs. For more details on the regional setting, see Liégeois et al. (1996).

The emplacement of the Tismana pluton has been dated at 567 ± 3 Ma (U–Pb zircon; Liégeois et al., 1996) and the twin Novaci pluton at 588 ± 5 Ma (U–Pb zircon; Grünenfelder et al., 1983). This study focuses on the shoshonitic Tismana pluton, nicely exposed (300 km^2; Fig. 2) and studied in detail (Berza, 1978). It was emplaced in the amphibolite facies Lainici-Păiuş Group. Both at small and medium scale, the contacts of the pluton are concordant with the schistosity of the country rocks. No apophyses or pluton-induced migmatites occur in the vicinity of Tismana, and only a few roof pendants of calc-silicate bearing marbles are found within the massif, close to the contacts.

3. A mafic–felsic association

The main rock types of the Tismana pluton (Fig. 2) are (1) a porphyritic granite, with K-feldspar megacrysts, containing abundant mafic enclaves and covering around 80% of the exposed area; (2) a darker equigranular facies, grading from diorite and uncommon gabbros to granodiorites and uncommon tonalites; the latter facies herein referred to as 'mafic rocks'. Pods of a few hundred metres of ultramafic rock outcrop in a restricted area. Although initially considered as a younger body (Berza, 1978), it actually belongs to the Tismana suite, the enclosing granite showing reaction and mingling structures at the contact (Tatu and Berza, 1994).

The distribution of the mafic rocks is systematic (Fig. 2). They prevail near the northwestern border, where they form a 1 to 1.5 km wide strip, here called the 'main mafic strip'. They are also common in the central part, where they occur as thinner strips or lenses with a maximum width of a few tens of metres and usually disposed in swarms. They are completely missing in the southernmost part of the exposed area. The grain size of these rocks also decreases southward: from 1–4 mm in the main mafic strip down to 0.3–0.5 mm in the smaller enclaves, which correspond to mafic microgranular (magmatic) enclaves (= MME; Didier and Barbarin, 1991).

K-feldspar megacrysts represent around 40% of the porphyritic granite. Assuming that they were floating, 40% of crystals in the melt would approach the limit between magmatic and submagmatic flow for acid magmas (Pitcher, 1993). The Tismana porphyritic granite commonly shows planar or swirling patterns similar to those described elsewhere (Nevez and Vauchez, 1995) and inferred to register magmatic flow with rigid body orientation of megacrysts or oblate enclaves. A free flow of K-feldspar megacrysts in the granitic magma is consistent with their trapping in blobs of coeval basic magma (Vernon, 1986).

4. A late-kinematic post-collisional pluton

The pluton induced a thermal effect on its metasedimentary envelope (Berza, 1978). According to $P–T$ grids (Spear, 1993), pressures around 2 kbar and temperatures around 600°C outside the body and over 800°C in the roof pendants are suggested.

The Tismana and Novaci massifs are late relative to the tectonics affecting the Lainici-Păiuş Group. The late effect of the tectonics on Tismana is marked by large (wavelength of 100 m to 1 km) symmetrical folding with vertical axial planes (Berza, 1978). A foliation, mainly NE–SW oriented and apparently not constrained by the pluton shape, is defined by: (a) oriented euhedral K-feldspar megacrysts in porphyritic granites; (b) oblate MME; (c) biotite orientation in mafic rocks of the main mafic strip. This foliation is parallel to the contacts between the porphyritic granite and the more mafic rocks and probably results from both magmatic flow and Pan-African regional tectonics. Despite Variscan and Alpine tectonics, these observations and the sheet-like emplacement of Tismana (Fig. 2) strongly suggest a late kinematic emplacement in a post-collisional setting, the collision being represented by the preceding amphibolite facies metamorphism.

Table 1

Major (%) and trace (ppm) element composition of representative samples of the Tismana pluton

Types	Peridotites		Mafic rocks							Intermediate rocks													Félsic rocks										
Group			G1		G1	G1				G2			G2			G3		G3			G3			G4	G4	G4	G4	G4	G4			G4	
Texture			m(1)	m						m	m	m		m																				
	R24	R650	R26	550	R12	504	826	1029	1143	R17	432	51	926	R27	52	1316	46	1264	375	1313	28	1265	430	53	927	1256	431	241	5	1311	827	1266	1267
SiO2	41.10	45.62	47.21	47.68	49.66	51.30	54.18	51.49	50.32	52.07	55.51	57.94	53.19	54.91	60.89	58.79	58.64	59.64	62.99	61.81	57.46	63.77	68.58	69.64	67.14	68.16	67.29	71.19	69.64	68.01	65.13	70.01	74.02
TiO2	0.17	0.45	1.64	1.78	1.20	1.70	1.53	1.25	1.53	1.80	1.85	1.41	1.94	1.56	1.22	1.56	1.51	1.40	1.17	1.17	1.72	1.11	0.91	0.65	0.64	0.70	0.71	0.49	0.59	0.68	0.39	0.56	0.05
Al2O3	4.31	7.87	16.97	16.87	16.82	17.00	16.04	17.94	17.95	16.39	14.84	16.11	15.24	16.21	15.78	15.37	15.68	15.48	14.33	15.41	14.75	14.22	13.03	14.04	15.13	14.57	14.88	13.50	14.01	14.74	17.31	14.38	13.58
Fe2O3t	13.12	11.61	11.08	10.42	10.32	8.62	9.10	9.38	11.24	11.41	10.08	8.07	11.43	9.86	7.36	8.39	8.22	7.87	6.63	6.77	10.04	6.02	5.41	3.05	3.78	4.06	4.62	3.28	3.64	3.95	1.85	3.56	0.98
MnO	0.16	0.16	0.17	0.16	0.15	0.14	0.15	0.16	0.19	0.19	0.16	0.11	0.16	0.16	0.10	0.13	0.12	0.11	0.09	0.08	0.16	0.08	0.07	0.04	0.07	0.04	0.05	0.04	0.04	0.05	0.03	0.03	0.03
MgO	32.48	23.83	7.18	6.73	6.51	5.69	4.87	4.61	4.42	3.34	3.31	2.85	2.76	2.71	2.59	2.57	2.18	2.11	1.89	1.87	1.84	1.61	1.39	1.11	1.08	1.07	1.03	0.84	0.80	0.79	0.78	0.48	0.29
CaO	1.00	4.17	7.71	8.43	7.95	6.60	7.19	5.73	5.91	5.43	5.55	4.19	5.17	4.52	4.57	4.22	4.11	3.77	3.23	3.47	4.48	3.04	2.01	1.56	1.93	2.16	1.80	0.61	1.46	1.87	1.68	1.52	0.69
Na2O	0.23	0.58	2.14	2.60	2.62	2.11	2.41	3.02	2.93	2.43	2.72	2.58	2.65	2.91	3.15	2.73	2.82	2.73	2.28	2.42	2.67	2.46	2.01	2.87	2.57	2.41	2.50	2.57	2.64	2.74	2.87	2.64	2.60
K2O	0.38	0.52	2.49	2.10	2.56	2.88	2.03	3.52	2.96	4.24	2.70	4.56	3.93	4.35	2.25	3.46	3.48	4.42	4.74	4.74	4.23	4.71	5.48	5.22	6.63	5.42	5.63	5.62	5.73	5.46	7.75	5.46	6.16
P2O5	0.02	0.03	0.77	0.71	0.73	0.54	0.61	0.60	1.00	1.03	0.62	0.49	1.01	0.79	0.39	0.48	0.81	0.48	0.60	0.41	0.98	0.36	0.39	0.20	0.23	0.35	0.32	0.24	0.23	0.28	0.13	0.20	0.02
LOI	7.00	4.43	2.40	2.40	1.86	2.73	2.60	1.98	1.62	1.46	1.14	1.25	1.67	1.55	1.34	1.73	1.47	1.62	1.20	1.48	1.04	1.72	1.33	1.25	0.98	0.96	1.31	1.29	1.25	1.32	1.15	1.19	0.71
Total	99.97	99.27	99.76	99.88	100.38	99.31	100.71	99.68	100.07	99.79	98.48	99.56	99.15	99.53	99.64	99.43	99.04	99.63	99.08	99.63	99.37	99.10	100.61	99.63	100.18	99.90	100.14	99.67	100.03	99.89	99.07	100.03	99.13
FeOt/FeOt+MgO	0.17	0.20	0.44	0.44	0.44	0.43	0.49	0.51	0.56	0.63	0.61	0.59	0.68	0.65	0.59	0.62	0.66	0.65	0.64	0.65	0.73	0.65	0.66	0.58	0.64	0.66	0.69	0.66	0.70	0.72	0.54	0.79	0.63
Agpaicity	0.18	0.19	0.37	0.39	0.42	0.39	0.38	0.49	0.45	0.52	0.50	0.57	0.57	0.59	0.48	0.54	0.54	0.60	0.61	0.59	0.61	0.64	0.71	0.74	0.75	0.67	0.69	0.76	0.75	0.71	0.76	0.71	0.81
U	0.4	0.4	1.6	1.1	1.4	1.2	0.4	0.3	1.4	2.0	1.0	0.8	0.4	1.6	1.1	1.3	1.8	1.7	3.3	1.4	1.8	2.9	2.8	2.0	1.4	2.0	1.8	3.0	1.8	2.1	0.9	3.8	2.3
Th	8.8	3.8	11.6	6.5	15.3	3.9	4.6	3.7	8.9	24.0	13.7	10.8	3.6	14.2	3.5	8.9	16.3	8.4	31.0	22.0	17.0	14.0	38.0	46.0	8.1	10.4	10.7	45.0	12.1	19.0	2.9	46.0	22.0
Th/U	24	11	7	6	11	3	11	12	6	12	14	14	8	9	3	7	9	5	10	15	9	5	14	23	6	5	6	15	7	9	3	12	10
Zr	51	47	236	300	322	305	337	265	224	519	547	517	472	442	425	336	659	545	745	554	732	560	504	376	364	402	424	355	341	329	191	336	90
Hf	1.6	1.4	7.9	6.5	7.0	7.0	7.7	5.6	4.5	12.4	13.8	12.6	10.8	10.5	10.0	9.8	17.9	14.4	18.6	14.3	15.1	13.9	12.2	9.1	9.1	9.7	10.0	8.6	8.0	8.1	3.4	7.7	3.0
Zr/Hf	33	34	30	46	46	44	44	47	49	42	40	41	44	42	43	34	37	38	40	39	48	40	41	41	40	42	42	41	43	41	57	44	30
Nb	2	2	59	60	69	52	49	53	89	92	73	57	102	70	42	51	75	59	61	62	93	47	47	28	39	35	36	42	36	37	18	43	4
Rb	22	41	98	94	107	167	76	143	106	151	171	153	122	153	140	131	173	152	178	165	123	141	205	158	167	158	225	225	227	256	203	229	178
Sr	44	203	688	740	1047	835	533	1281	1336	744	407	545	628	561	535	173	539	571	339	447	524	516	233	510	475	391	331	170	255	192	479	231	165
Ba	98	228	1135	1035	1497	1182	941	1478	1848	2014	1003	1522	2074	1864	703	1187	1252	1676	1251	1496	2009	1539	971	1522	1586	1462	1424	925	1006	807	2179	773	683
K/Rb	143	105	211	185	199	143	222	204	232	233	131	247	267	236	133	219	167	241	218	238	286	277	222	274	330	285	208	207	210	177	317	198	287
K/Ba	32	19	18	17	14	20	18	20	13	17	22	25	16	19	27	24	23	22	31	26	17	25	47	28	35	31	33	50	47	56	30	59	75
V	83	128	180	190	163	157	144	131	93	105		117	97	105	111	94	94	69	68	63	72	48	46	26	34	26	36	27	30	34	25	26	5.6
Cr	2548	2090	52	55	88	31	57	10	17	24	11		11	16	9	14	12	6	17	15	12	7	13	21	13	11	14	7	9	14	9	9	7
Zn	88	91	106	112	99	102	122	84	108	132	134	91	151	120	94	98	102	107	93	97	132	79	82	43	55	59	69	56	46	69	35	57	0
Co	118	91		32	37	26	27	32	25	27	25	19	22	20	12	21	10	16	9	16	14	17	7	4	3	10	15	2	15	8	1	20	22
Ga				19	22	22	19	17				23	23	24	23	20	22	21	22	24	22	20	21	18	20	20	22	20	22	23	21	20	15
Pb	6	7	17	11	5	12	12	11	14	21	8	17	17	27	11	17	16	13	22	34	22	17	23	21	22	21	23	27	19	21	24	25	35
Y	7	16	35	34	35	36	37	25	33	46	65	43	60	43	40	53	37	46	44	57	25	31	16	23	19	27	38	22	25	9	21	28	
La	14	8	70	75	90	66	62	92	154	130	120	87	89	112	46	69	108	74	143	92	162	77	109	176	59	63	67	116	71	76	29	86	27
Ce	14	14	134	138	182	116	130	150	204	266	229	162	198	227	96	129	241	154	283	178	301	153	213	321	109	115	130	204	131	146	48	158	64
Nd	7	9	60	59	77	49	62	58	74	119	110	75	97	90	52	54	97	73	107	81	116	61	88	103	46	45	50	74	48	59	18	62	25
Sm	1.3	2.5	11.3	12.0	11.9	8.4	10.8	8.4	10.6	17.9	20.0	14.0	16.0	14.4	9.7	9.4	16.4	11.7	15.7	14.2	18.0	8.9	13.6	11.3	7.7	6.6	8.0	14.0	7.6	9.4	2.7	9.3	5.0
Eu	0.35	0.60	3.03	2.90	2.72	2.35	2.67	2.60	3.15	3.20	3.00	2.90	3.68	2.98	2.04	2.67	2.83	2.70	2.67	2.59	3.43	2.29	1.74	2.08	2.22	2.16	1.78	1.52	1.63	1.63	2.33	1.50	1.06
Gd		2.3	9.4	8.8	9.9	7.1	9.1	6.6	8.2	14.5	16.0	10.8	13.8	15.9	7.8	7.4	13.4	9.2	12.3	10.8	15.1	6.7	10.1	7.8	6.0	5.4	6.1	9.7	5.6	7.5	1.9	7.3	3.1
Tb	0.17	0.38	1.26	1.20	1.30	0.94	1.28	0.87	1.10	1.94	2.42	1.53	2.01	1.67	1.14	0.97	1.85	1.26	1.61	1.50	2.05	0.84	1.28	0.78	0.83	0.59	0.78	1.24	0.68	1.00	0.20	0.83	0.58
Dy	0.97	2.19	6.31	5.80	6.17	5.05	6.40	4.40	5.40	9.25	12.40	7.65	10.40	8.08	5.64	5.17	8.76	6.14	6.90	7.41	10.40	4.23	5.75	2.69	4.24	3.20	3.84	5.96	3.61	4.74	1.13	4.15	3.03
Er	0.60	1.27	3.30	3.20	2.96	2.67	3.43	2.35	2.86	4.30	6.28	3.95	5.46	4.03	3.41	2.88	4.91	3.25	3.65	3.75	5.44	2.23	2.71	1.19	2.14	1.75	2.10	3.26	1.92	2.13	0.78	1.84	3.16
Yb	0.65	1.21	3.02	2.90	2.83	2.41	3.02	2.23	3.00	3.88	5.26	3.53	4.96	3.89	3.70	2.82	4.61	3.00	3.47	3.57	5.09	2.35	2.32	1.23	2.15	1.67	1.85	3.02	1.73	1.82	0.67	1.59	4.61
Lu	0.10	0.20	0.55	0.50	0.49	0.33	0.44	0.32	0.48	0.64	0.77	0.49	0.75	0.63	0.48	0.39	0.58	0.38	0.44	0.48	0.78	0.30	0.36	0.18	0.31	0.24	0.27	0.50	0.21	0.25	0.08	0.22	0.79
La/Yb n		4	15	15	21	18	13	27	33	12	22	15	16	12	19	8	16	15	16	27	17	21	30	93	18	24	23	25	26	27	28	35	4
Eu/Eu*	1.43	0.76	0.88	0.83	0.76	0.91	0.81	1.04	1.01	0.60	0.50	0.70	0.75	0.60	0.70	0.57	0.78	0.57	0.62	0.62	0.88		0.44	0.65	0.98	1.09	0.76	0.38	0.74	0.82	3.04	0.54	0.78

(1) m: microgranular texture.

(1) m: microgranular texture.

Sample location, petrographic name and, in brackets, the geochemical name after Debon and Le Fort (1988). R24 and R650: Ultramafic cumulate, Fintina valley; R26 and 550: Microgranular diorite (monzogabbro), Giula valley; R12: Diorite (monzogabbro), Mare valley; 504: Quartz diorite (quartz monzodiorite), Mare valley; 826: Quartz monzodiorite (quartz monzodiorite), Frasin valley; 1029: Quartz diorite (monzonite), Petru valley; 1143: Diorite (quartz monzonite), Runcu valley; R17: Microgranular enclave (quartz monzonite), gallery tailings, Pocrula valley; 432: Microgranular inclusion (quartz monzodiorite), Pocruia valley; 51: Microgranular enclave (quartz monzonite), Tismana valley; 926: Quartz monzodiorite (quartz monzonite), Bistricioara valley; R27: Microgranular enclave (quartz monzonite), Giula valley; 52: Granodiorite (granodiorite), Tismana valley; 1316: Tonalite (adamellite), Runcu valley; 46: Tonalite (granodiorite), Tismana valley; 1264: Granodiorite (quartz monzonite), Petru valley; 375: Biotite and hornblende porphyritic granite (granite), Poiana cu Fragi valley; 1313: Granodiorite (granite), Runcu valley; 28: Granodiorite (quartz monzonite), Pocruia valley; 1265: Biotite and hornblende porphyritic granite (granite), Petru valley; 430: Granite (granite), Tismanita valley; 53: Porphyritic granite (granite), Tismana valley; 927: Porphyritic granite (granite), Bistricioara valley; 1256: Porphyritic granite (granite), Mare valley; 431: Porphyritic granite (granite), Pocruia valley; 241: Porphyritic granite (granite), Paltinei valley; 5 and 1311: Porphyritic granites (granites), Pocruia valley; 827: Porphyritic granite (quartz syenite), Frasin valley; 1266: Porphyritic granite (granite), Neguroasa valley; 1267: Aplite (granite), Neguroasa valley.
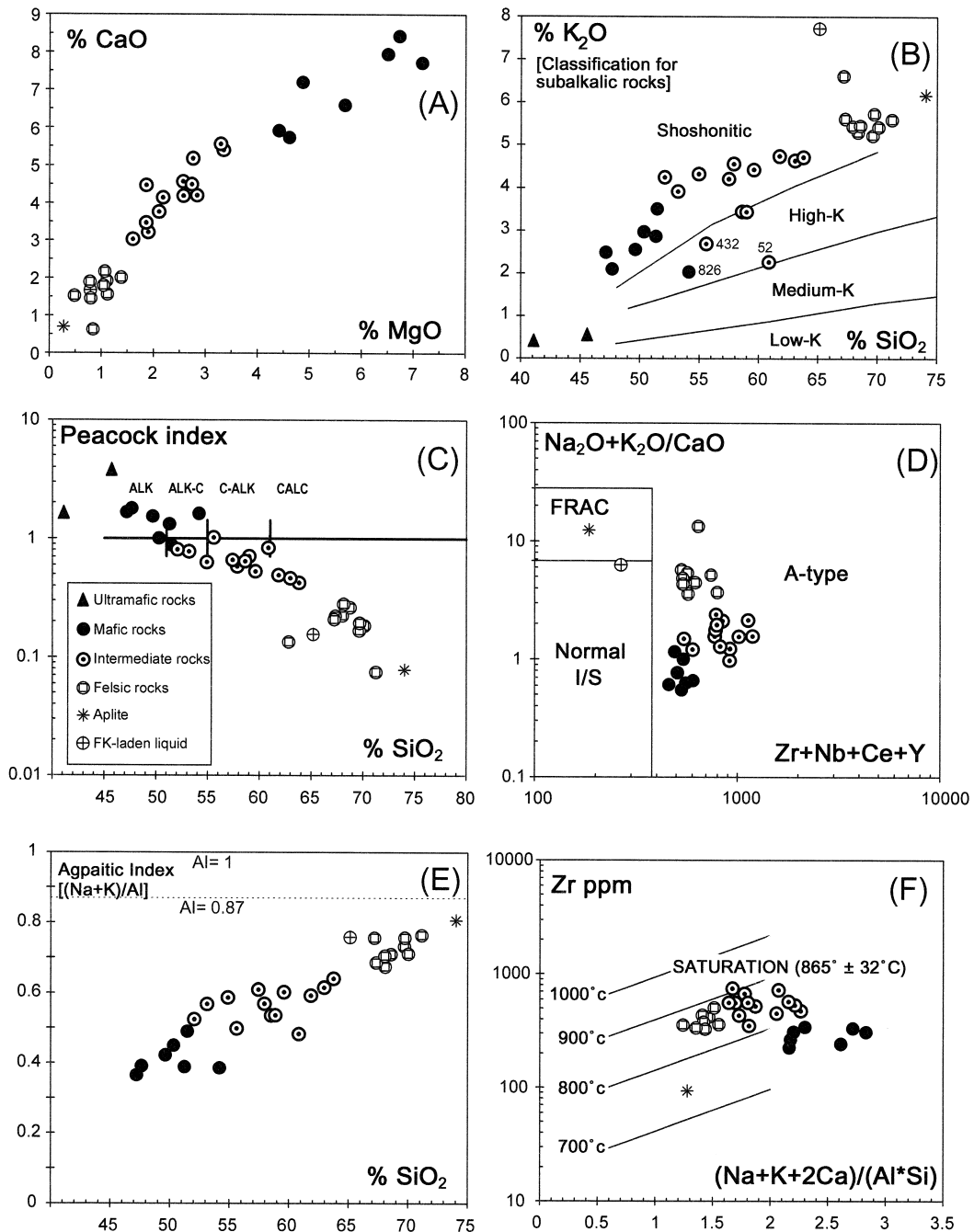
Fig. 3. Selected geochemical characteristics of the Tismana shoshonitic series (legend for rock types in C). (A) CaO vs. MgO; (B) K_2O vs. SiO_2; the dividers are after Rickwood (1989); (C) Peacock index ($CaO/(Na_2O + K_2O)$) vs. SiO_2 after Brown (1981); (D) $CaO/Na_2O + K_2O$ vs. $Zr + Nb + Ce + Y$ after Whalen et al. (1987); (E) Agpaitic index $(Na + K)/Al$ (atom%) vs. SiO_2. The limit at AI = 0.87 (minimum value for alkaline meta-aluminous granitoids) is after Liégeois and Black (1987); (F) Zr vs. $(Na + K + 2Ca)/Al * Si$ after Watson and Harrison (1983); zircon saturation isotherms are indicated; the average zircon saturation temperature (865°C) is calculated for the felsic rocks and the intermediate rocks with the X parameter < 2.

5. Tismana granitoids: petrography and mineralogy

Tismana felsic and mafic rocks show clear evidence of mingling and mixing processes, as described elsewhere (Vernon, 1986; Didier and Barbarin, 1991; Pitcher, 1993). They have given rise to a hybrid porphyritic granodioritic facies. For clarity of the petrographic description, we have distinguished four distinct rock types although progressive transitions between all of them are witnessed by field evidence: (1) the porphyritic granite; (2) the equigranular mafic rocks; (3) the hybrid granodioritic facies; (4) the ultramafic rock.

5.1. The porphyritic granite

The Tismana porphyritic granite is a coarse-grained rock characterized by abundant (40%) oriented white-grey euhedral K-feldspar megacrysts up to 12 cm in length (with a mean of 3–4 cm). The groundmass is made up of plagioclase, quartz, microcline, biotite, scarce hornblende and abundant accessory minerals (ilmenite, apatite, zircon, titanite, allanite). The K-feldspar is a perthitic maximum microcline ($Or_{70}Ab_{30}$; Berza, 1978). The K-feldspar megacrysts contain abundant plagioclase inclusions whose {010} planes are parallel to those of their host. Plagioclase crystals are much smaller (~ 2–3 mm),
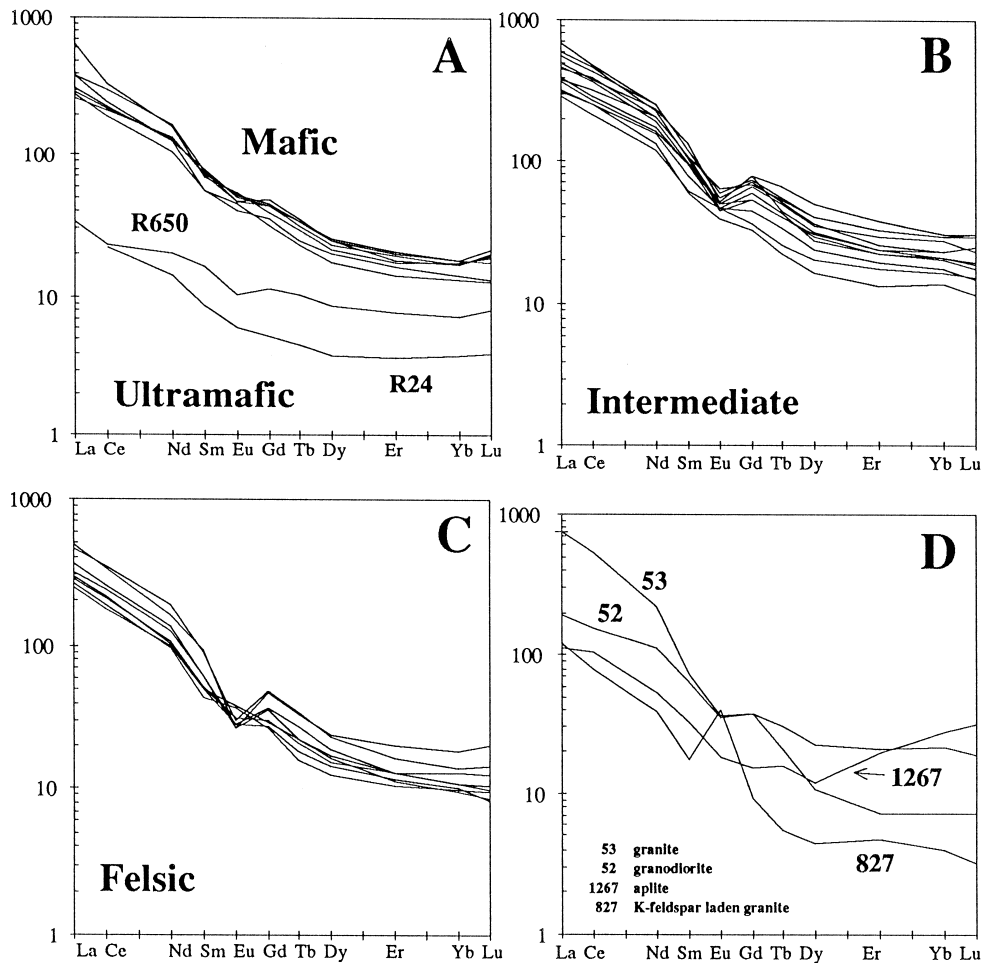
Fig. 4. Chondrite-normalized REE distribution. (A) Ultramafic and mafic rocks; (B) Intermediate rocks; (C) Felsic rocks, main stream (without 52); (D) Atypical samples 827 (K-feldspar laden porphyritic granite), 1267 (aplite), 52 (granodiorite) and 53 (porphyritic granite).
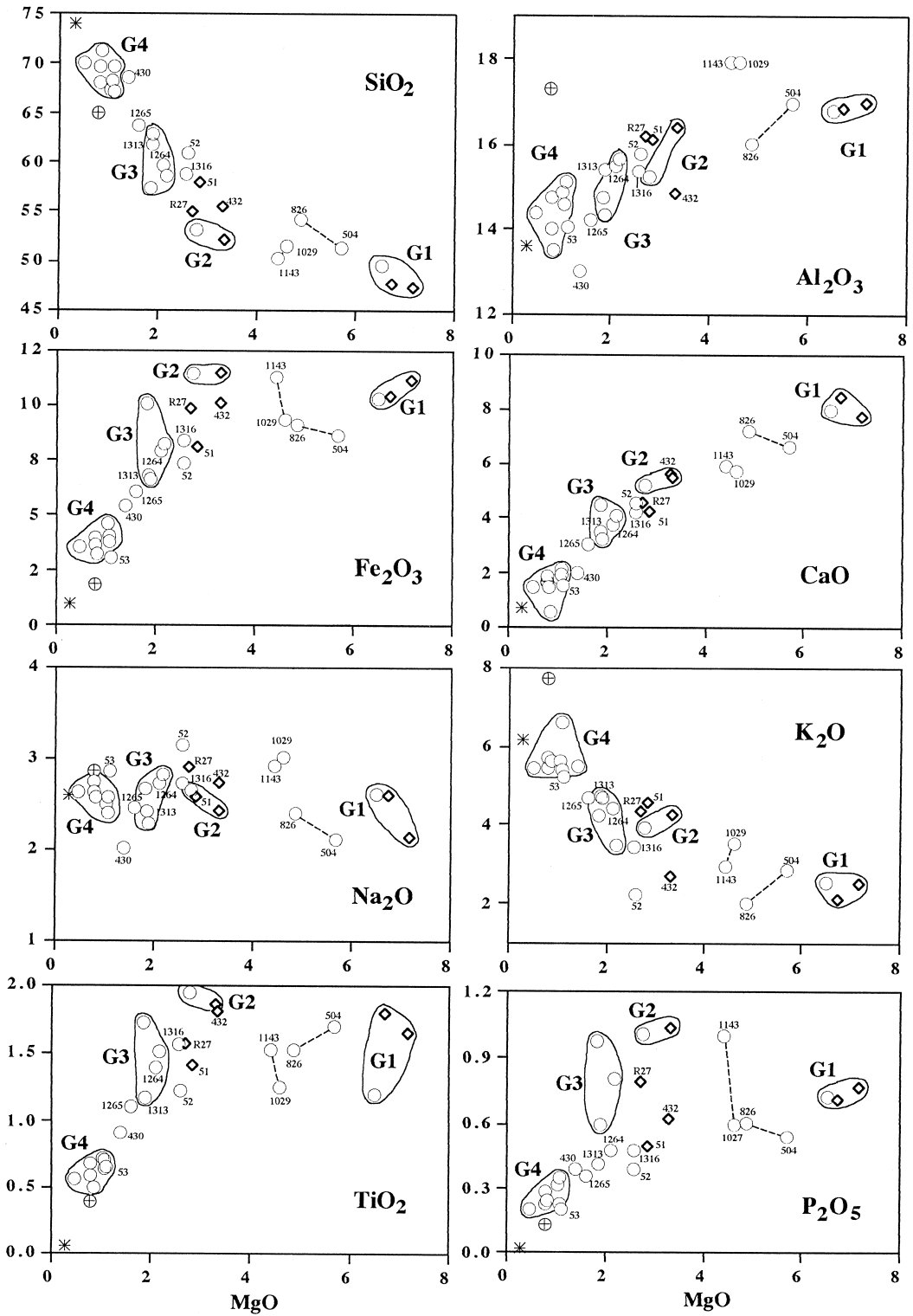
mostly euhedral. Generally An_{28-30} in composition, they are more calcic (An_{36}) when hornblende is present (hybrid facies, see below). Biotite is red-brown, euhedral and contains most of the accessory minerals. It has an mg no. ($Mg/(Mg + Fe^{2+} + Mn)$) between 0.34 and 0.43 and a TiO_2 content around 3.4%. Some hastingsitic brown-olive hornblende (mg no. 0.37) occurs locally. The colour index of the typical Tismana granite is between 10 and 15, rather high for granite. Aplites appear in numerous dykes (sample 1267).

5.2. The mafic rocks from the strips and enclaves

In the main mafic strip, the mineral grain size is nearly constant ($\sim$ 1–3 mm). Variations on the scale of a few metres of the quartz and intergranular K-feldspar contents shift the rocks from diorite to tonalite, granodiorite or quartz monzodiorite with a constant high mafic mineral content (35–45%). Biotite is always present whereas the hornblende and clinopyroxene contents vary considerably. Orthopyroxene is locally present, giving rise to noritic varieties, a unique feature in the South Carpathians. The rock is either massive or, more commonly, has a fabric, biotite defining a foliation plane.

Plagioclase is euhedral and its composition varies from An_{32-40} in granodiorites and quartz monzodiorites to a mean of An_{52} for gabbros or norites. K-feldspar is interstitial. The mg no. of biotite diminishes from 0.90 (ultramafic rock) to 0.40 (granite). The amphibole mg no. in the granodiorite averages 0.42 (Berza, 1978). Clinopyroxene can form up to 25% of the more mafic rocks. Orthopyroxene, commonly altered to bastite, grades from $En_{66}Fs_{32}Wo_2$ in norites to $En_{57}Fs_{41}Wo_2$ in quartz norites (Berza, 1978). In diorites and quartz diorites, apatite is the most abundant accessory. Zircon and rutile are ubiquitous. Ilmenite is the characteristic opaque mineral, representing up to 3–4% of the rock.

5.3. The hybrid granodioritic facies

This transitional facies is porphyritic, with randomly oriented K-feldspar megacrysts, typical of the granite, and with amphibole and locally clinopyroxene, which are characteristic minerals for the MME. For similar reasons developed by authors who studied similar plutons (e.g., Nevez and Vauchez, 1995), including field observations, we consider this facies as resulting from hybridisation (complete mixing) of mafic and porphyritic granite melts. Moreover, in the regular porphyritic granite, there are zones several hundred metres wide which contain amphibole in addition to biotite and a plagioclase some 7% richer in anorthite than is the case in the main granitic mass. This facies is also considered as hybrid.

5.4. The ultramafic rock

The most mafic rocks in Tismana are olivine-bearing cumulates, outcropping as a few lenses of several hundred metres in the centre of the pluton, a unique occurrence in South Carpathians plutons. This fine-grained ($\sim$ 2–3 mm) rock contains 40–45 modal% olivine oikocrysts (Fo_{82-84}), 15–20% interstitial orthopyroxene (mg no. 0.86–0.90), 10% brown phlogopite (mg no. 0.85–0.90), 5–10% brown amphibole (mg no. 0.81–0.84) and less than 10% plagioclase. Accessory minerals are pyrrhotite with pentlandite exsolutions, and titanomagnetite. Olivine is commonly altered into a mixture of smectite and chlorite. In some places, clinopyroxene coexists with orthopyroxene. Oikocrysts of olivine are devoid of deformation features, and far from the contacts with olivine, orthopyroxene and phlogopite are commonly euhedral. Even if the whole rock normative composition is harzburgitic, the general characteristics of these ultramafic lenses are typical of alkaline cumulates. According to Edgar (1987), the olivine + orthopyroxene + phlogopite association is at the liquidus of K-rich magmas with 5% H_2O below 15

Fig. 5. Major element content (%) vs. MgO content (see Table 1). Legend: ○ (open circle) unspecified rocks; ◇ (diamond): microgranular rock;) ⊕ (open circle with cross): porphyritic granite, sample no. 827 (K-feldspar laden melt); ∗ (asterisque): aplitic granite no. 1267; G1 to G4 refer to groups of rocks which show similar geochemical characteristics (see text and Table 2). Dashed lines connect samples considered together in the modelling.
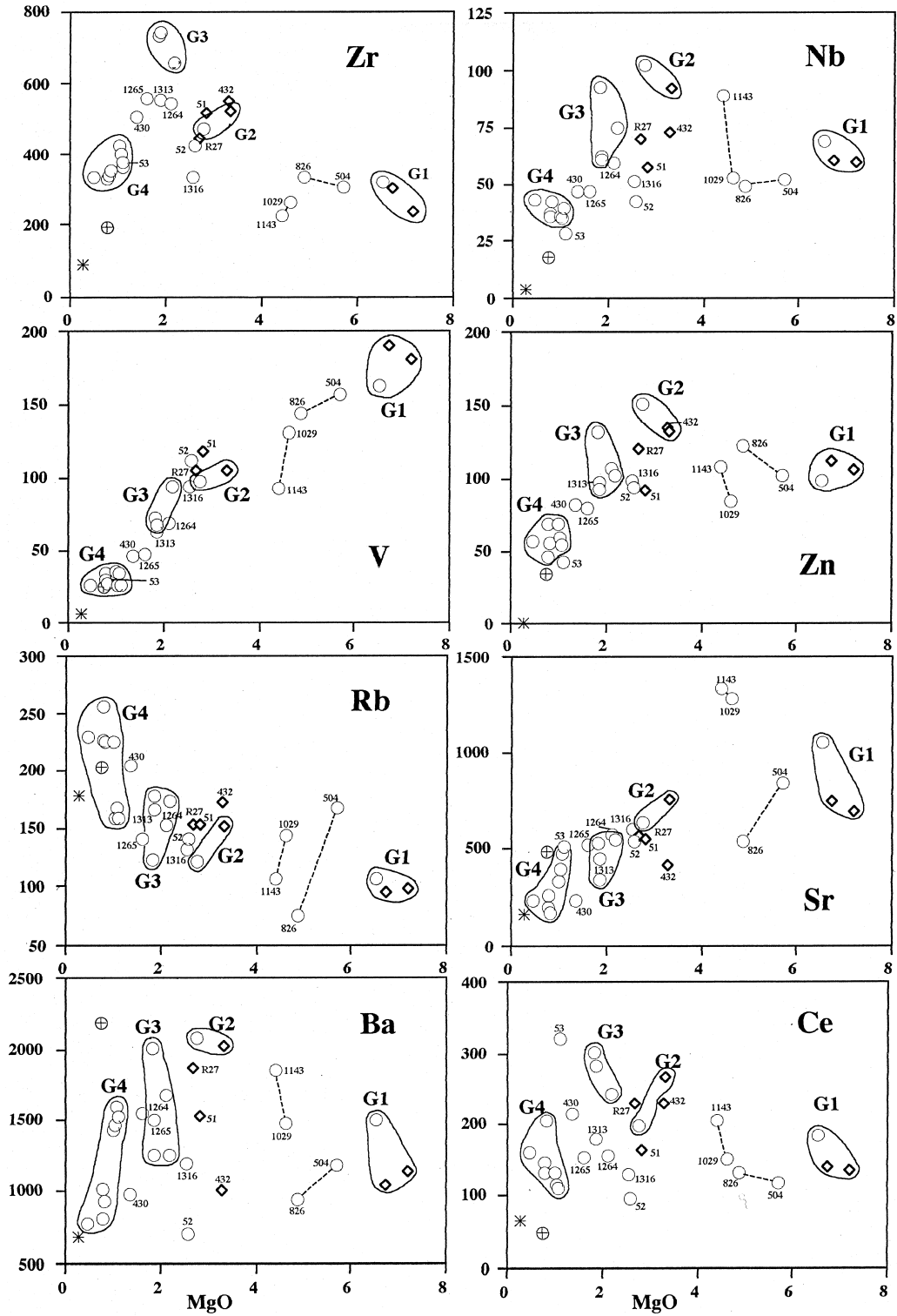
kbar. A discussion of this occurrence will be published elsewhere (Latouche et al., in preparation).

6. Geochemical modelling

Major and trace element analyses of 33 representative samples of the pluton, including six microgranular enclaves (MME), are reported in Table 1 and plotted in Figs. 3–6. The analytical methods are briefly described in annex.

6.1. Main characteristics

Four main groups of rocks can be distinguished on the basis of the MgO and CaO contents (Fig. 3A; Table 1) in order to simplify the discussion: (1) the ultramafic cumulates (24–33% MgO); (2) the mafic rocks (7.5% to 4.5% MgO); (3) after a small gap in MgO, the intermediate rocks (3.5–1.7% MgO) and (4) the felsic rocks (1.5–0.5% MgO) separated from the intermediate rocks by a small gap in CaO (Fig. 3A).

The Tismana pluton forms a continuous shoshonitic series from 50% to 75% SiO_2 (Fig. 3B; Le Maitre, 1989; Rickwood, 1989). It is worth mentioning that the Tismana trend mimics the classical shoulder (transition from mafic to intermediate rocks) defined for the lower boundary of the shoshonitic field. This trend is alkali-calcic (Peacock index; Brown, 1981: Fig. 3C). The shoshonitic character is accompanied by high contents of some incompatible elements not linked to an alkaline affinity even if the Tismana trend is falling into the A-type domain of the widely used diagram of Whalen et al. (1987; Fig. 3D). Indeed, the agpaitic index reaches a value of only 0.8 in the most acid rocks (Fig. 3E), far from peralkalinity or even from the minimum value of metaluminous granites belonging to the alkaline series (0.87; Liégeois and Black, 1987). One obvious difference between the Tismana and the alkaline series is that Tismana has low Na_2O contents (2–3% from 47% to 74% SiO_2) and in turn high K_2O/Na_2O ratios (1.5 to > 2 for intermediate and felsic rocks).

Structural data (see above) preclude an anorogenic setting, and the mineralogy is not anhydrous (biotite and amphibole are ubiquitous as well as subsolvus feldspars). None of the A-characters that would support an A-type suite according to the original definition is present. Consequently, Tismana cannot be considered as an A-type suite nor as a transalkalic suite: it shares only some common geochemical characteristics with A-type series, as a result of its shoshonitic signature.

A relatively high temperature of crystallization, around 865°C, is given by the saturation of zircon (Fig. 3F; Watson and Harrison, 1983). Indeed, after an increase within the mafic rocks, Zr reaches its maximum content within the intermediate rocks. It is only from this point that the zircon thermometer gives liquidus values.

The incomplete mixing and mingling patterns observed at all scales everywhere in the Tismana pluton point to a complex geochemistry. Indeed, all elements (except V, CaO) show a variable spreading in variation diagrams (see below, Figs. 5 and 6). In the best cases, rough trends can be observed (e.g., Rb and K increase with the decrease of MgO). Only diadochic elements behave in a consistent way (Table 1): Zr/Hf has an average of 41 ± 5 and La_N/Yb_N varies between 12 and 35 (with the exception of ultramafic cumulates, granite 5 and aplite 1267; Table 1); K/Rb (grossly) and K/Ba (strongly) increase towards acid rocks (Table 1). U and Th contents as well as Th/U ratios vary more erratically (Table 1) with values between 4 and 12. Large Th variations occur within a single facies (e.g., from 2.9 ppm to 46 ppm in the porphyritic granites) whereas other trace elements are more homogeneous (e.g., Ta from 1.2 to 4.8 ppm). This could be due to some heterogeneity in the distribution of Th(-U)-bearing accessory phases or/and to the supergene mobility of U.

As discussed below, REE patterns show evidence of fractional crystallization, of mixing between different facies and of local accumulation of feldspar. However, all spectra share a common signature: (high REE content and similar La/Yb ratios) which strongly point to a consanguineous origin and similar

Fig. 6. Selected trace element contents (ppm) vs. MgO content (see Table 1). Same legend as in Fig. 5.

evolution. Ultramafic cumulates (Fig. 4A) have low REE abundances, an enrichment in LREE ($La_N/Yb_N = 4$–6) and a small negative Eu anomaly or none. Mafic rocks (Fig. 4A) are remarkably very enriched in LREE ($La_N = 170$–400; La_N/Yb_N: 14–33) and the negative Eu anomaly is small or absent ($Eu/Eu*$: 1.04 to 0.76). The main stream in the intermediate rocks (Fig. 4B) is slightly more enriched in REE ($La_N = 105$–309) but the La_N/Yb_N ratio is somewhat smaller (12–22) and the Eu negative anomaly is pronounced (average $Eu/Eu* = 0.68 \pm 0.13$). Felsic rocks show grossly the same characteristics as intermediate ones (average $La_N/Yb_N = 26 \pm 5$; average $La_N = 238 \pm 62$, $Eu/Eu* = 0.69 \pm 0.25$; Fig. 4C), except for an aplite (1267), a K-feldspar laden magma (827 with an $Eu/Eu* = 3$), an atypical granite (53, $La_N/Yb_N = 97$; Fig. 4D) and a granodiorite (52) with a peculiar low K_2O content.

6.2. Modelling a liquid line of descent

When the fractional crystallization trend of a given element is close to a straight line in a variation diagram, the possible effect of a mixing between basic and acid members will generally increase the linear character of the trend, and the two processes will be difficult to distinguish (Provost and Allègre, 1979). On the other hand, when the trend is curved or bell-shaped (as in the case of incompatible elements which increase up to saturation), mixing between any liquid on the trend can dramatically disperse the data points inside the concavity of the fractional crystallization trend. This blurring effect can make the interpretation more intricate. Nevertheless, if samples are properly chosen, the actual differentiation trend—the liquid line of descent—can be delineated. These selected samples have to be quantitatively modelled, while the others must fit into a mixing framework. Our selection was based on the following points: (1) in the mafic rocks, homogeneous microgranular rocks are preferentially considered because they are the best candidates to represent liquid compositions; (2) the most basic ones are selected as representing the parent magma; (3) samples reaching maxima in P_2O_5, TiO_2 and Zr contents (classical incompatible elements) are considered as belonging to the liquid line and to reach

saturation in apatite, ilmenite and zircon, respectively; (4) among the felsic rocks, a series of samples of similar composition in some elements or showing a short evolution trend for others have been chosen. Based on these criteria the samples that belong to the liquid line of descent have been divided into four groups (G1 to G4; Figs. 5 and 6; Tables 1 and 2).

6.2.1. The G1 group (R26, 550 and R12)

The first two samples are microgranular diorite forming large (> 1 m, up to 50 m) inclusions in the southern part of the pluton (Fig. 2). The third sample comes from the main mafic strip in the NW of the massif. In most variation diagrams, the three samples are closely grouped. The microgranular texture, the non-porphyritic character and the similarity in composition of these rocks suggest crystallization from a melt, considered here as the parent magma.

6.2.2. The G2 group (R17, 926)

R17 is a microgranular quartz diorite enclave and 926 a coarser-grained quartz monzodiorite. Both samples have similar composition in all elements and display maximum values in P_2O_5, TiO_2, Nb, Zn, and Ba.

6.2.3. The G3 group (28, 46, 375)

Samples 28 and 46 are two granodiorites and 375 a hornblende-bearing porphyritic granodiorite (35). G3 is characterized by maximum values in Zr and REE contents.

6.2.4. The G4 group (5, 241, 431, 927, 1256, 1266, and 1311)

They are porphyritic granites, which display similar values in Zr, Nb, TiO_2 or short evolutionary trends for Rb, Ba and P_2O_5.

A consistent body of evidence supports the four groups as defining a liquid line of descent.

(1) *Liquidus minerals in G1*. Taking the FeO value of 7.44% in sample 550 (from Table 8 of Berza, 1978) and using the method of calculation of Ford et al. (1983), the temperature and composition of olivine in equilibrium with G1 are 1220°C and Fo_{84} (at 3 kbar). Similarly, application of the MIXNFRAC3 algorithm (Nielsen, 1988) to simulate the crystallization of G1 at a f_{O_2} at FMQ (the FeO and Fe_2O_3 contents were calculated at FMQ, 1220°C and

Table 2
Average composition of the various groups of rocks

	G1	G2	G3	G4
SiO_2	48.18	52.63	59.70	68.78
TiO_2	1.54	1.87	1.47	0.62
Al_2O_3	16.89	15.82	14.92	14.46
Fe_2O_3t	10.61	11.42	8.30	3.84
MnO	0.16	0.18	0.12	0.05
MgO	6.81	3.05	1.97	0.87
CaO	8.03	5.30	3.94	1.62
Na_2O	2.45	2.54	2.59	2.58
K_2O	2.38	4.09	4.13	5.71
P_2O_5	0.74	1.02	0.80	0.26
LOI	2.22	1.57	1.24	1.19
Total	100.01	99.47	99.16	99.98
FeOt/FeOt + MgO	0.44	0.65	0.68	0.69
Agpaicity	0.39	0.54	0.59	0.72
U	1.4	1.2	2.3	2.3
Th	11	14	21	22
Th/U	8	10	9	9
Zr	286	496	712	364
Hf	7	12	17	9
Zr/Hf	41	43	42	42
Nb	63	97	76	38
Rb	100	137	158	212
Sr	825	686	467	292
Ba	1222	2044	1504	1140
K/Rb	198	250	223	231
K/Ba	16	17	24	44
V	178	101	78	30
Cr	65	12	14	11
Zn	106	142	109	59
Co	35	24	11	10
Ga	19	12	22	21
Pb	11	19	20	23
Y	35	53	52	25
La	78	110	138	77
Ce	151	232	275	142
Nd	65	108	107	55
Sm	12	17	17	9
Eu	2.9	3.4	3.0	1.8
Gd	9.4	14.2	13.6	6.8
Tb	1.25	1.98	1.84	0.85
Dy	6.1	9.8	8.7	4.2
Er	3.15	4.88	4.67	2.16
Yb	2.92	4.42	4.39	1.98
Lu	0.51	0.70	0.60	0.29
La/Yb n	17	17	21	25
Eu/Eu *	0.82	0.67	0.59	0.72

3 kbar using the regression of Kress and Carmichael, 1991: FeO = 7.98% and Fe_2O_3 = 1.99%) shows that, at 1193°C, Fo_{85} is the only phase present at the liquidus, a composition in close agreement with the previous calculation. This calculated composition for olivine closely matches the measured composition of this mineral in ultramafic cumulates (Fo_{82} to Fo_{84}). This strongly suggests that the olivine of this cumulate has crystallised from a liquid close to G1. At 1161°C, olivine (Fo_{81}) is joined by plagioclase (An_{70}) and, at 1080°C, augite (Wo_{43} En_{41} Fs_{16}) appears and coexists with Fo_{68} and An_{60}. At the latter temperature, the residual liquid is close in composition to G2, but differs by higher contents in CaO and Fe_2O_3. This difference can be accounted for by a higher augite proportion in the subtracted assemblage, as shown by a least square calculation (Table 3 cumulate no. 1). The fraction of 0.13 augite compared to 0.02 in Nielsen's calculation can be explained by some intercumulus augite crystallised from entrapped liquid in the liquidus assemblage (orthocumulate). The fraction of residual liquid at this stage is 0.58. Consistently, incompatible elements, such as Zr, Nb and the REE, increase by approximately a factor of 2 during this stage of evolution. Similarly, transition elements (e.g., V, Cr, Co) decrease because they are strongly partitioned into the mafic minerals.

(2) *Liquidus minerals in G2*. Further modelling by Nielsen's approach of the liquid line of descent has not been performed because hydrous phases like biotite and hornblende (minerals not taken into account in the simulation of MIXNFRAC3) appear on the liquidus of more evolved stages. Instead, we have used a least square regression method (Table 3). In order to evolve towards G3, which is lower in P_2O_5 than G1, G2 has to be saturated in apatite. According to Harrison and Watson (1984), this saturation will take place around 1000°C. Subtraction of a cumulate containing Plag (An_{45}) + Bt (mg no. 0.72) + Aug (mg no. 0.65) + Ilm (Hem_3) + Mt (5% TiO_2) + Ap, in which the clinopyroxene and biotite compositions were taken according to respective compositions measured in dioritic rocks (Berza, 1978), gives an acceptable residue (r^2 = 0.14). Due to subtraction of apatite in which REE are enriched, the REE become compatible and decrease further in the liquid evolution. Similarly, decrease in Zn can be

Table 3

Modelling of the three differentiation stages of the Tismana liquid line of descent

Stage 1[a]

	Plag (An_{60})	Ol (Fo_{68})	Aug * (mg no. = 0.70)
SiO_2	53.40	36.27	50.69
TiO_2	0.00	0.00	0.50
Al_2O_3	29.70	0.00	3.60
Fe_2O_3	0.00	30.75	10.55
MgO	0.00	32.97	13.34
CaO	12.10	0.00	21.19
Na_2O	4.80	0.00	0.00
K_2O	0.00	0.00	0.00
P_2O_5	0.00	0.00	0.00

Stage 2[b]

	Plag * (An_{45})	Biot * (mg no. = 0.72)	Aug (mg no. = 0.65)	Ilm (Hem_3)	Magn	Ap
SiO_2	57.30	36.90	41.75	0.49	1.74	0.00
TiO_2	0.00	3.25	0.50	48.81	4.84	0.00
Al_2O_3	27.10	15.77	10.55	0.39	3.10	0.00
Fe_2O_3	0.00	22.44	13.84	49.67	87.75	0.00
MgO	0.00	12.97	13.71	0.55	0.46	0.00
CaO	9.00	0.00	19.25	0.10	0.11	54.80
Na_2O	6.10	0.00	0.00	0.00	0.00	0.00
K_2O	0.50	8.67	0.00	0.00	0.00	0.00
P_2O_5	0.00	0.00	0.00	0.00	0.00	41.70

Stage 3[c]

	Plag (An_{30})	Biot * (mg no. = 0.38)	Horn * (mg no. = 0.43)	Ilm (Hem_3)	Ap
SiO_2	61.00	34.86	39.24	0.49	0.00
TiO_2	0.00	3.48	1.59	48.81	0.00
Al_2O_3	24.70	16.31	10.59	0.39	0.00
Fe_2O_3	0.00	29.61	27.81	49.67	0.00
MgO	0.00	7.24	6.46	0.55	0.00
CaO	6.10	2.01	10.42	0.10	54.80
Na_2O	7.20	0.00	1.20	0.00	0.00
K_2O	1.00	6.46	2.09	0.00	0.00
P_2O_5	0.00	0.00	0.00	0.00	41.70

[a] From G1 to G2. MIXNFRAC3 algorithm of Nielsen (1988): $T = 1193°C$, Fo_{85}, $F = 0.99$; $T = 1161°C$, $Fo_{81}An_{70}$, $F = 0.96$; $T = 1080°C$, $Fo_{68}An_{60}Aug(Wo_{43}En_{41}Fs_{16})$, $F = 0.58$. At $T = 1080°C$, the subtracted assemblage is 0.32 Ol + 0.66 Plag + 0.02 Aug. Least square regression method: cumulate no. 1: 0.60 An_{60} + 0.27 Ol + 0.13 Aug; Σr^2 (sum of squared residues) = 1.7 F_1 (fraction of residual liquid) = $f = 0.46$.

[b] From G2 to G3. Least square regression method: cumulate no. 2: 0.42 An_{45} + 0.36 Biot + 0.07 Aug + 0.02 Ilm + 0.08 Mag + 0.05 Ap. $\Sigma r^2 = 0.14$; $F_2 = 0.66$, $f = 0.30$.

[c] From G3 to G4. Least square regression method: cumulate no. 3: 0.39 An_{30} + 0.14 Biot + 0.40 Hornb + 0.04 Ilm + 0.03 Ap. $\Sigma r^2 = 0.20$; $F_3 = 0.65$, $f = 0.20$.

* From Berza, 1978.

explained by crystallization of magnetite and decrease in Ti and Nb by crystallization of ilmenite. The subtracted assemblage is a meladiorite. Similar assemblages and bulk compositions have their counterparts in diorite massifs (e.g., Traversella: van

Marcke de Lummen and Vander Auwera, 1990). The high mafic content is not surprising: mafic-rich cumulates (with apatite and oxides at the liquidus) are also known in layered intrusions (such as the Bjerkreim–Sokndal intrusion; Wilson et al., 1996)

and their occurrence as liquidus assemblages has been confirmed experimentally (Vander Auwera et al., 1998).

(3) *The final stage from G3 to G4.* Subtraction of a cumulus assemblage containing biotite (mg no. 0.38) and hornblende (mg no. 0.43) with compositions currently found in the most basic granodiorites (Berza, 1978; Table 3) together with ilmenite, apatite and andesine mimics the observed evolution. Zr evolution culminates in G3, which indicates that zircon is at saturation in that liquid. According to Watson and Harrison (1983), zircon should precipitate at $865 \pm 32°C$ in G3 (Fig. 3), a reasonable liquidus temperature for such potassic melts. The presence of zircon in the liquidus assemblage together with apatite, whose partition coefficients for REE should be larger than in the previous stage due to the increase in the silica content of the liquid (Watson and Green, 1981), induces a decrease of the REE content from G3 to G4 (Fig. 6). Zircon precipitation would also explain the increase in the La_N/Yb_N from 21 in G3 to 25 in G4. Transition elements continue to decrease due to the subtraction of mafics. Ba and Zn also decrease, as a consequence of biotite crystallization (Ba up to 3000 ppm in biotites separated from granodiorites; Berza, 1978; Zn up to 1240 ppm; Corriveau, 1989). Rb increases with differentiation, indicating that K-feldspar at liquidus was not abundant enough to decrease the Rb content, thus permitting the liquid to keep high K_2O contents.

Sample 1267 (aplite) has unique characteristics: it is the most evolved rock (extreme values in all major elements, and the lowest Zr, Hf, Nb, V, Cr, Zn, Sr, Ba contents). Rb is slightly depleted compared to the most evolved granites, possibly due to very late K-feldspar crystallization. The average REE are low and the distribution shows a typical enrichment in HREE, which is not uncommon for aplite (e.g., van Marcke de Lummen and Vander Auwera, 1990) or for highly evolved granites in which titanite has crystallised (e.g., Cocherie et al., 1994).

6.3. Mixing between liquids and the role of cumulative K-feldspar

We have tested the hypothesis that some samples that plot inside the bell-shaped liquid line of descent correspond to mixing between two different liquids taken among the four groups defined above (G1 to G4). Moreover, some samples are considered as liquids laden with some excess K-feldspar. For this purpose, proportions of the two end-members have been calculated by mass balance on the major elements using multiple regression techniques. Results indicate that the average of samples 826 and 504 can be accounted for by mixing of 78% G1 and 22% G4. Sample 1316 contains a more important proportion of G4: 52% of G4 and 48% G1, whereas the average composition of samples 51 and R27 is explained by the mixing of 74% G2 and 26% G4. Finally, the average of samples 1313, 430, 1264 and 1265 corresponds to the mixing of 59% G3 and 41% G4. The same mixing calculations have also been performed with trace elements, using the fraction of the end-members calculated from the major elements. The range of differences between calculated element content and the observed one is shown in Fig. 7 as a function of Z^2R, where Z is the valence and R the ionic radius. As noted by Hofmann (1980), the diffusivity or mobility of a cation in a melt decreases with increasing ionic charge and size, and is negatively correlated with the empirical Z^2R value. Fig. 7 indicates that (1) except for Th and U, the agreement between observed and calculated values is good and supports the hypothesis of a bulk mixing; (2) the large discrepancy observed for Th is not observed for its neighbour Nb. It cannot, therefore, reflect heterogeneity in the melts due to low diffusivity of this element.

We have used a similar approach to test that several granites are laden with K-feldspar. The porphyritic granite 827, characterized by a strong positive Eu anomaly, high Al_2O_3, K_2O and Ba contents together with low REE contents, is likely to represent the G4 liquid laden with 46% K-feldspar. Granites 927 and 1256 which display no Eu anomalies and are enriched in Ba (Table 1) possibly correspond to a G4 liquid in which 8% K-feldspar has accumulated. Note that granitic samples only are laden with K-feldspar, which confirms that this mineral began to crystallise belatedly.

All other samples are localised inside the polygon formed by G1 to G4 and can be considered as mixtures between liquids generated at various stages of the evolution along the liquid line of descent.
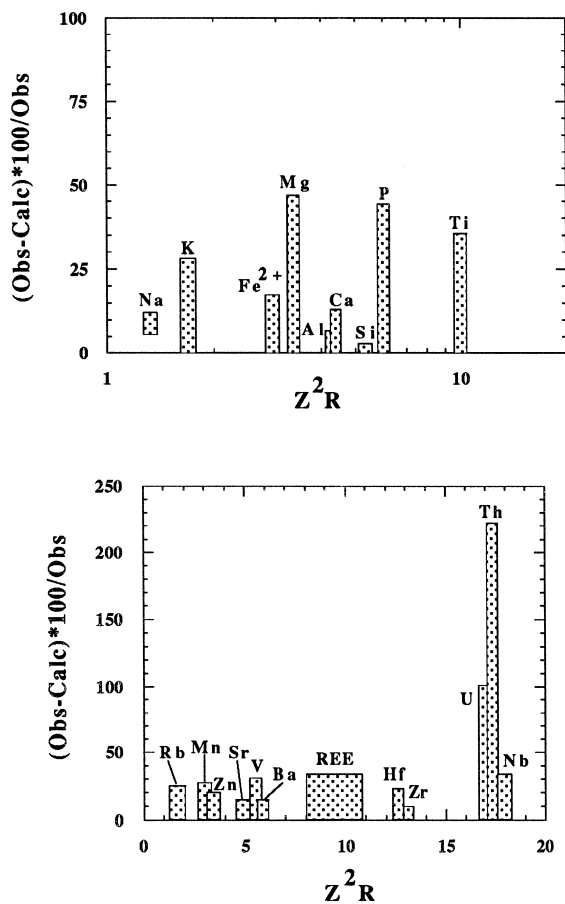
Fig. 7. Difference between observed and calculated contents in major and trace elements of sample 1316 or of several groups of samples $(826 + 504, 51 + R27, 1313 + 430 + 1264 + 1265)$ which possibly represent hybrid compositions (see text for explanation). The range of differences are expressed as relative percent of the observed compositions and shown as a function of the relative diffusivity (Z^2R; Hofmann, 1980). Z is the ionic charge and R, the ionic radius. Ionic radii are taken from Whittaker and Muntus (1970), assuming octahedral coordination for all cations except Si and Al, for which tetrahedral coordination has been considered. A $+3$ oxidation state was chosen for V and a $+2$, for Fe.

Several of them are microgranular enclaves (432, 27, 51), in which 432 shows the petrographic characteristics of a chilled liquid (apatite with high aspect ratio). This points to a complete mixing process at a temperature above the liquidus temperatures.

In conclusion, the complex mixing process, well displayed in the field, is translated in the geochemistry. However the characteristic feature is that the melts that mix together are not two distinct unrelated magmas but derive from the same parent magma. It can therefore be called endo-hybridisation. The original liquid line of descent can be reconstructed, showing a complete evolution from diorite to granite by crystal fractionation. The ultramafic cumulate contains an olivine in equilibrium with the most basic parent liquid. This one ($\sim 50\%$ SiO_2), as well as the associated ultramafic cumulate, are already enriched in K_2O (3% in dioritic liquid; primary phlogopite in the ultramafic rock). This implies that the source was already enriched in K_2O.

7. Isotopic constraints for a crustal contamination

Recalculated back to 567 Ma (U–Pb zircon age; Liégeois et al., 1996), the Sr and Nd isotopic ratios form a trend ($Sr_i/\varepsilon Nd$) from mafic ($0.7065/-2.5$) to felsic rocks ($0.712/-6$; Table 4; Fig. 8A), suggesting a combined assimilation/fractional crystallization process (AFC; DePaolo, 1981). The crustal contaminant having to be older than 1100–1500 Ma, as indicated by the T_{DM} model ages (Table 4). However, when looking at silica vs. initial ratios (Fig. 8B,C), the global trend appears less regular, particularly within each group: e.g., during the differentiation of intermediate rocks, the Sr and Nd initial ratios are rather stable. A simple binary mixing between a mafic magma and a felsic magma— already invoked in the geochemical modelling—can explain the composition of two samples (52 and 1316, hybrid rocks) only, as particularly well shown by Nd vs. SiO_2 in Fig. 8D but also by Sr (Fig. 8E,F). Such a mixing process however does not explain the Nd contents of the other samples: the Nd concentrations in the intermediate rocks are higher than in both the mafic and the felsic samples (incompatible before apatite saturation and compatible afterwards; Fig. 8D, inset), a feature already highlighted in the geochemical modelling. On the other hand, the apparent regular increase of Sr_i with the decrease of Sr is only roughly related to the differentiation index (Fig. 8E and inset), particularly in the mafic rocks. Actually, each element which behaves regularly with silica (e.g., CaO; Fig. 8F) displays a rough correlation with Sr_i from the means of mafic to that of the

Table 4
Sr and Nd isotopes

Group	No.	Rb	Sr	$^{87}Rb/^{86}Sr$	$^{87}Sr/^{86}Sr$	$2\sigma m$	$Sr_i = 567$ Ma	Sm	Nd	$^{147}Sm/^{144}Nd$	$^{143}Nd/^{144}Nd$	$2\sigma m$	ε_{Nd}	T_{BE}	T_{DM}
Ultramafic	R24	22	44	1.4482	0.71659	0.000013	0.704883	1.31	6.5	0.1219	0.512385	0.000029	0.49	516	1094
Ultramafic	R650	41	203	0.5847	0.711434	0.000010	0.706708	2.49	9.4	0.1600	0.512398	0.000010	−2.03	998	1824
Mafic	550	94	740	0.3677	0.710434	0.000011	0.707462	12.00	59	0.1230	0.512127	0.000008	−4.63	1057	1535
Mafic	R12	107	1047	0.2958	0.708879	0.000010	0.706488	11.85	77	0.0936	0.512124	0.000006	−2.56	760	1166
Mafic	1029	143	1281	0.3231	0.709441	0.000010	0.706829	8.40	58	0.0876	0.512090	0.000028	−2.79	766	1152
Intermediate	52	141	535	0.7632	0.715165	0.000010	0.708995	9.68	52	0.1126	0.512094	0.000008	−4.52	986	1427
Intermediate	432	173	407	1.2315	0.719887	0.000014	0.709932	19.00	102	0.1126	0.512051	0.000008	−5.37	1064	1493
Intermediate	926	121	620	0.5651	0.714384	0.000011	0.709816	15.30	93	0.0995	0.512046	0.000010	−4.51	928	1329
Intermediate	R17	151	744	0.5877	0.714073	0.000011	0.709322	17.90	119	0.0910	0.512012	0.000007	−4.56	903	1279
Intermediate	R27	153	561	0.7898	0.715516	0.000019	0.709131	14.40	90	0.0968	0.511954	0.000004	−6.11	1043	1417
Intermediate	1316	131	595	0.6375	0.713507	0.000011	0.708354	9.40	54	0.1053	0.512080	0.000012	−4.27	930	1352
Intermediate	28	123	524	0.6798	0.715688	0.000011	0.710193	18.00	116	0.0938	0.512007	0.000013	−4.86	935	1316
Intermediate	46	176	542	0.9405	0.716705	0.000009	0.709102	16.40	97	0.1022	0.512076	0.000013	−4.12	907	1321
Felsic	431a	225	331	1.9711	0.728221	0.000008	0.712287	7.97	50	0.0964	0.511984	0.000018	−5.50	994	1374
Felsic	1256	158	391	1.1709	0.720672	0.000019	0.711207	6.58	45	0.0884	0.511948	0.000007	−5.62	971	1331

T_{BE} and T_{DM} (in Ma), calculated following parameters of Nelson and DePaolo (1985). ε_{Nd} calculated at 567 Ma.
Rb, Sr, Sm, Nd concentrations are in ppm.
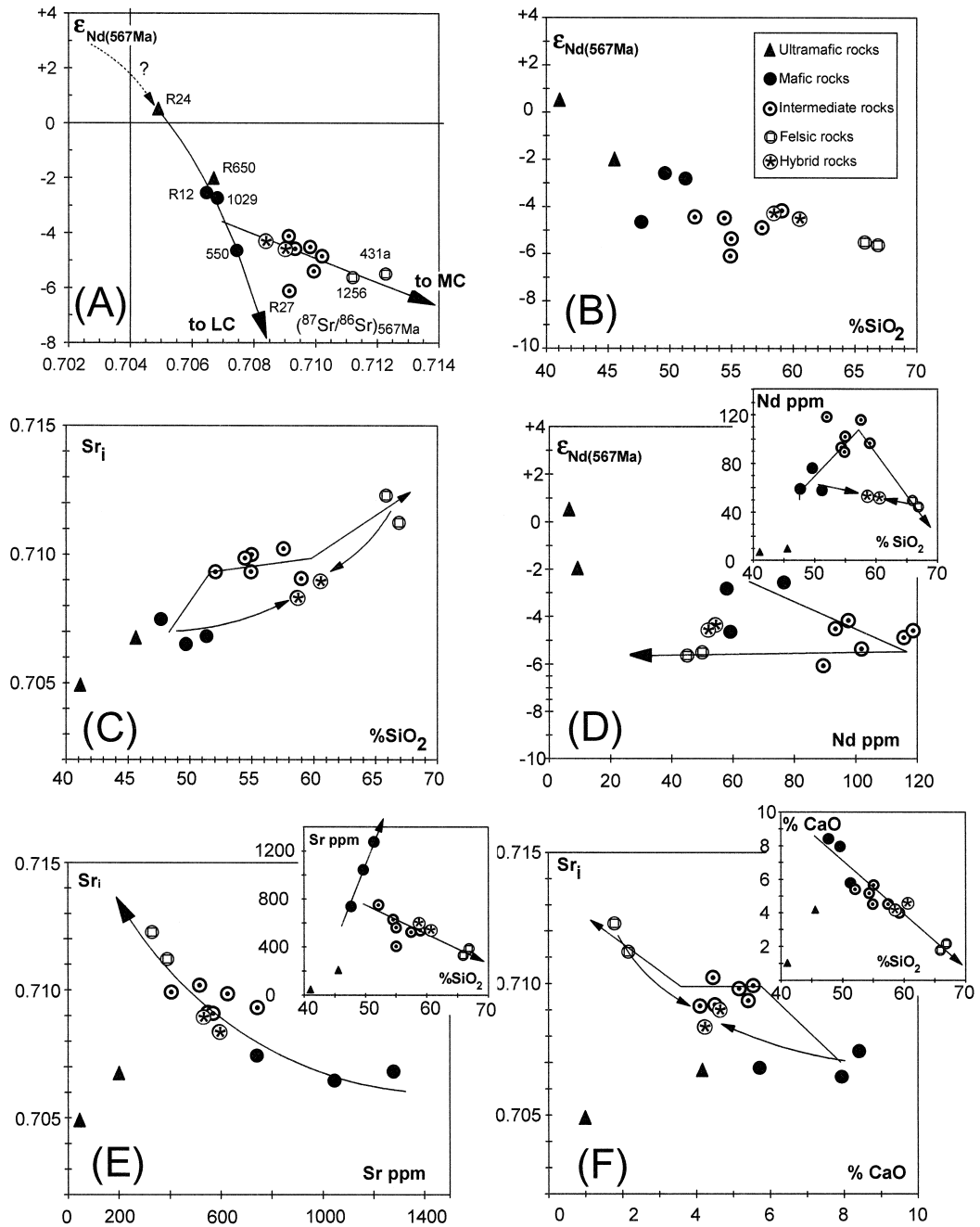
Fig. 8. Isotopic characteristics of the Tismana series (Sr and Nd isotopic ratios calculated back to 567 Ma, the zircon age; Liégeois et al., 1996). Legend for rock types are in (B) Intermediate rocks were formed by fractional crystallization while hybrid rocks were formed by mingling between mafic and felsic rocks: (A) ε_{Nd} vs. Sr_i. LC means lower crust and MC medium crust; (B) ε_{Nd} vs. SiO_2; (C) Strontium isotope initial ratio (Sr_i) vs. SiO_2; the broken arrow shows the differentiation trend, while the two other arrows show the formation of the hybrid rocks by mixing. (D) ε_{Nd} vs. Nd; inset: Nd vs. SiO_2; (E) Sr_i vs. Sr; inset: Sr vs. SiO_2; (F) Sr_i vs. CaO; inset: CaO vs. SiO_2. Data in Tables 1 and 4.

felsic rocks, but detailed correlations show the constancy of initial ratios within the intermediate rocks.

Two trends can be decrypted within the Tismana bi-isotopic diagram (Fig. 8A): from the ultramafic cumulates (which have been in isotopic equilibrium with a liquid) to the mafic samples, there is an important decrease in ε_{Nd} (from $+0.5$ to -4.6) for a moderate increase in Sr_i (from 0.7049 to 0.7075), while from intermediate to felsic rocks there is mainly an increase in Sr_i (0.7084 to 0.7123 for -4.1 to -5.6 in ε_{Nd}, excluding R27 at -6.1). This points to a Rb-depleted lower crust as the first contaminant and to an undepleted medium crust for the second. Sample R27 seems to indicate that some intermediate rocks could have also suffered an additional lower crustal contamination (Fig. 8A). Additional data, including oxygen isotopes, are needed, however, to precise the respective role of lower and mid crusts.

An attempt to quantify this process needs the definition of these contaminants; they cannot be determined for the Tismana pluton, which belongs to a thin Alpine thrust. However, Liégeois et al. (1996) have proposed links with the Pan-African Tuareg shield (Central Sahara) where a potassic leucogranite of regional extension has been described (Renatt granite; Liégeois et al., 1994). This Renatt crustal granite resulted from a widespread regional melting of the Archaean lower crust and interacted in many places with the amphibolite facies mid crust. It thus provides an excellent average for the less refractory felsic components of both the lower and mid crusts (FLC and FMC, respectively). Average of FLC and FMC can then be set up (Liégeois et al., 1994). FLC: $Sr_i = 0.71038$, $\varepsilon_{Nd} = -22.1$, $Sr = 80$ ppm, $Nd = 15.6$ ppm; FMC: $Sr_i = 0.74468$, $\varepsilon_{Nd} = -19.1$, $Sr = 187$ ppm, $Nd = 24.4$ ppm.

AFC equations, mainly developed by DePaolo (1981), have been recently extended by Aitcheson and Forrest (1994) to allow independent estimation of the r value (crust/magma ratio in non-recharge situations) for different isotopes or elements. Taking both Sr and Nd isotopes, it is possible to vary the r value (rate of assimilation of crust/rate of fractional crystallisation) to obtain an identical r for both isotopes (Aitcheson and Forrest, 1994). An alternative approach would assume a selective contamination due to decoupling of isotopes and elements (Lesher,

1990) but, in this case, few constraints can be given (Roberts and Clemens, 1995, 1997). We used here the Eq. (5) of Aitcheson and Forrest (1994), which is the most complete one, and the partition coefficients based on the calculated cumulate compositions derived from the Tismana major element modelling (within G1 and from G1 to G2: $D_{Sr} = 1.17$ and $D_{Nd} = 0.376$; from G2 to G3: $D_{Sr} = 1.46$ and $D_{Nd} = 0.831$; from G3 to G4: $D_{Sr} = 2.15$ and $D_{Nd} = 1.66$).

Evolution from mafic to felsic rocks implies the use of the FMC parameters (Fig. 8A). This gives a crustal participation of 13.7% from G1 to G2, of 0% from G2 to G3 (they have indeed the same Nd and Sr initial ratios) and a maximum of 4.5% from G3 to G4. The low values of the contamination do not significantly alter the major element modelling presented above, inasmuch as the process could be selective for the isotopes (Baker, 1989; Lesher, 1990). For the early evolution, to explain the variation during the formation of the ultramafic cumulates, we must contaminate the G1 group with an FLC contaminant. This gives a crustal participation of 33% from R24 to 550. Such a high contamination by a felsic component is, however, unrealistic from a heat budget point of view and moreover would drastically change the major element composition, which is not the case (e.g., sample 550 has 47.7% SiO_2). This suggests that the contaminating lower crust was also of mafic composition. To further evaluate this hypothesis, we use the Sr and Nd concentrations of the parental magma of the Bjerkreim–Sokndal lopolith in Norway, the Tjörn monzonorite (530 ppm and 39 ppm, respectively; Duchesne and Hertogen, 1988), without changing the Nd and Sr isotopic ratios typical anyway for an old lower crust. The calculation gives rise to a contamination of 23%, but with slight major element modifications, as the Tjörn monzonorite composition is not very different from that of the Tismana (monzo)diorites.

8. Constraints on the source of the Tismana shoshonitic series

The trend observed in the ε_{Nd} vs. Sr_i diagram indicates that the source of the Tismana shoshonitic series had a $Sr_i < 0.7049$ and an $\varepsilon_{Nd} > +0.5$, as

suggested by the dotted arrow (Fig. 8A). These constraints point to a mantle or to a juvenile mafic lower crust enriched or formed not a long time before Tismana. In the first case, a strong interaction (e.g., an acceptable 23% contamination) with an old mafic lower crust is needed, while in the second case, the mafic lower crust could be composed of alternating juvenile and old dioritic layers. In both cases, the mantle source of Tismana or of the juvenile lower crust, had to be enriched in K_2O and associated elements. This could result from a subduction-related enrichment of the lithospheric mantle during the Pan-African orogeny. The 800 Ma old Dragşan oceanic island arc in the South Carpathians basement (Liégeois et al., 1996) could reflect this subduction.

Experimental works indicate that K_2O metasomatism of the mantle wedge overlying the subduction zone can produce mantle phases such as phlogopite or K-richterite (Schmidt, 1996), and relict subduction zones are seen by seismic reflection profiles in old lithospheric mantle (Warner et al., 1996). Substantial participation of a lithospheric mantle, previously enriched in LILE stocked in refractory phlogopite, has been invoked as the source of potassic magmas in China (Zhang et al., 1995) and in Tibet (Turner et al., 1996).

Partial melting of such a formerly refractory source (either lithospheric mantle or layered mafic lower crust) implies an extra heat supply which could be brought about by a rapid asthenospheric upwelling, such as in Tibet or in Aïr, possibly due to lithospheric delamination (England and Houseman, 1989; Black and Liégeois, 1993). All these features are consistent with an extensional post-collisional setting for Tismana.

9. The magma chamber and emplacement scenario

The structure of the massif and the petrological and geochemical data put several constraints on the differentiation and emplacement mechanisms. Several liquids of different composition corresponding to various stages of fractional crystallization have to be present simultaneously in the actual magma chamber to account for mingling structures and microgranular enclaves. No particular mafic cumulates stuck against wall rocks are observed that could explain the evolution towards acidic rocks (McBirney et al., 1985) within the Tismana pluton itself. It can thus be concluded that neither wall–rock segregation nor crystal fractionation by gravity were operating in the chamber represented by the actual pluton. Another magma chamber (at least) at greater depth (> 2 kbar) is thus required to develop a compositionally zoned magma column, grading towards the roof of the chamber to the most evolved granite. This chamber could be compared to, e.g., the mid-crustal Bjerkreim–Sokndal layered intrusion (Wilson et al., 1996). A selective or a mild isotopic contamination with a felsic medium crust has taken place in this chamber.

During the formation of the ultramafic cumulates —in a first magma chamber or in the conduit through the lower crust—Nd and Sr isotopes indicate either a strong interaction between a mantle mafic magma with an older mafic lower crust or the partial melting of a layered lower crust comprising mafic juvenile and older rocks. The latter situation can easily occur in a post-collisional setting, the preceding subduction and/or collision having the opportunity to incorporate juvenile mafic material into the lower crust. Finally, en route to the actual Tismana chamber, the Tismana felsic rocks might also have suffered an additional slight contamination with the crust. In the Tismana chamber, observed mingling and mixing processes between mafic and felsic magmas generated hybrid rocks of intermediate composition, but with peculiar geochemical and isotopic characteristics when compared to differentiated intermediate rocks.

Before complete crystallization, the two deep-seated chambers were deformed due to late tectonic post-collisional movements. This deformation tapped the magma chambers from the top: the granitic liquid (in which phenocrysts of K-feldspar had already crystallized) intruded a shallower magma chamber (the actual pluton), together with less evolved liquid drawn from lower zoned parts, to form the main mafic strip, lots of strips and countless enclaves. Stirring and mingling were active during the emplacement. Finally, as the initial magma chamber was more and more reduced in size, some of the bottom cumulates, still incompletely crystallised (the

ultramafic cumulates), were dragged and squeezed into the shallower chamber, the Tismana pluton.

10. Conclusions

Though complex and partly enigmatic, the petrological and geochemical characters of the Tismana pluton point to several patent features.

(1) A liquid line of descent, linking dioritic (monzodioritic) liquids to granites can be reconstructed, which indicates that the granitic end-member is derived from the former by fractional crystallization, with only slight crustal contamination, but not from the partial melting of a distinct sialic source.

(2) Several influxes of parent magmas have taken place since the parent liquid (or less evolved, or most basic liquid) is found as inclusions in the more evolved melts.

(3) Mixing occurred between parent liquid and granitic melt, as well as between liquids at various stages of evolution, which could be called endo-hybridisation; total mixing was possible above liquidus temperature.

(4) Though porphyritic, the granite is likely to represent a liquid, sorting and accumulation of K-feldspar phenocrysts being very local.

(5) The ultramafic cumulate is a cognate inclusion, its olivine being in equilibrium with the parent liquid.

(6) Nd and Sr isotopes show that the most mafic rocks could have suffered a relatively high contamination (ca. 23%) by an old mafic lower crust, while more evolved rocks could have been contaminated by a felsic medium crust (from 15% for the intermediate rocks to 4% for the felsic rocks).

(7) Based on these constraints, a model requiring at least two magma chambers is built up. In the high-level chamber (the actual pluton) only mingling/mixing occurred. The deep seated chamber, in which most of the evolution takes place including contamination with mid-crustal material, can be compared to the Bjerkreim–Sokndal intrusion. Crystallization of the ultramafic cumulate and lower crustal isotopic contamination can possibly develop in the early conduit.

(8) the Sr and Nd isotopic initial ratios of the parent magma of the Tismana shoshonitic pluton indicate that its source was either a K_2O-enriched lithospheric mantle or a juvenile mafic layered lower crustal source deriving partly from such a mantle. This enrichment could have taken place during the preceding Pan-African subduction period. Its partial melting soon after its generation may be due to a mantle delamination.

(9) The main characteristics of the Tismana plutons, viz. composition, contamination, magma chambers succession and relation with regional tectonics, all point to a post-collisionnal setting; in particular, its source, either the mantle or a juvenile mafic lower crust, requires modifications or generation during the just preceding collision or subduction period.

Appendix A. Analytical techniques

Isotopic measurements were carried out on a Fisons VG Sector 54 mass spectrometer. Repeated measurements of Sr and Nd standards have shown that between-run error is better than 0.00002. The NBS987 standard has yielded a value for $^{87}Sr/^{86}Sr$ of 0.710263 ± 0.000005 during this study (2s on the mean, normalised to $^{86}Sr/^{88}Sr = 0.1194$) and the

MERCK Nd standard a value for ^{143}Nd/^{144}Nd of 0.512722 ± 0.000006 (2s on the mean, normalised to ^{146}Nd/^{144}Nd = 0.7219). Decay constants used (Steiger and Jäger, 1977) are 1.42×10^{-11} a^{-1} (^{87}Rb), and $6.54 \ 10^{-12}$ a^{-1} (^{147}Sm). For more details, see Liégeois et al. (1996).

XRF on Li borate and carbonate (with La) glass discs was used to determine major elements, except Na, measured on pressed raw material, and FeO, determined by titration (Bologne and Duchesne, 1991). Two different techniques were used for the analysis of 26 trace elements: XRF on raw material for Rb, Sr, Zn, Nb, and V (Bologne and Duchesne, 1991); ICP-MS for all the other elements (Vander Auwera et al., 1999)

References

Aitcheson, S.J., Forrest, A.H., 1994. Quantification of crustal contamination in open magmatic systems. J. Petrol. 35, 461–488.

Baker, D.R., 1989. Tracer versus trace element diffusion: diffusional decoupling of Sr concentration from Sr isotope composition. Geochim. Cosmochim. Acta 53, 3015–3023.

Berza, T., 1978. Studiul mineralogic si petrografic al masivului granitoid de Tismana. An. Inst. Geol. Geof. 53, 1–176.

Black, R., Liégeois, J.-P., 1993. Cratons, mobile belts, alkaline rocks and continental lithospheric mantle: the Pan-African testimony. J. Geol. Soc. London 150, 89–98.

Bologne, G., Duchesne, J.C., 1991. Analyse des roches silicatées par spectrométrie de fluorescence X: précision et exactitude. Belgian Geol. Survey Prof. Paper 249, 1–11.

Bonin, B., Platevoet, B., Vialette, Y., 1987. The geodynamic significance of alkaline magmatism in the western Mediterranean compared with West Africa. In: Bowden, P., Kinnaird, J.A. (Eds.), African Geology Reviews, Geol. J. Thematic Issue 22, 361–387.

Brown, G.C., 1981. Space and time in granite plutonism. Philos. Trans. R. Soc. London, Ser. A 301, 321–336.

Cocherie, A., Rossi, P., Fouillac, A.M., Vidal, P., 1994. Crust and mantle contributions to granite genesis: an example from the Variscan batholith of Corsica, studied by trace element and Nd–Sr–O isotope systematics. Chem. Geol. 115, 173–211.

Corriveau, L., 1989. Proterozoic potassium-rich alkaline plutonism in the southwestern Grenville Province. PhD thesis, McGill University, Montreal, Canada.

Debon, F., Le Fort, P., 1988. A cationic classification of common plutonic rocks and their magmatic associations: principles, method, applications. Bull. Minéral. 111, 493–510.

DePaolo, D.J., 1981. Trace element and isotopic effects of combined wallrock assimilation and fractional crystallization. Earth Planet. Sci. Lett. 53, 189–202.

Didier, J., Barbarin, B., 1991. Enclaves and granite petrology. Development in Petrology 13, Elsevier, Amsterdam.

Duchesne, J.C., Hertogen, J., 1988. Le magma parental du lopolithe de Bjerkreim–Sokndal (Norvège méridionale). C. R. Acad. Sci. Paris 306, 45–48.

Edgar, A.D., 1987. The genesis of alkaline magmas with emphasis on their source region: inferences from experimental studies. In: Fitton, J.G., Upton, B.G.J. (Eds.), Alkaline Igneous Rocks, The Geological Society, Blackwell, pp. 29–52.

England, P.C., Houseman, G.A., 1989. Extension during continental convergence, with application to the Tibetan plateau. J. Geophys. Res. 94, 17561–17579.

Ford, C.E., Russell, D.G., Craven, J.A., Fisk, M.R., 1983. Olivine–liquid equilibria: temperature, pressure and composition dependence on the crystal/liquid cation partition coefficients for Mg, Fe^{2+}, Ca and Mn. J. Petrol. 24, 256–265.

Grünenfelder, M., Popescu, G., Soroiu, M., Berza, T., 1983. K–Ar dating of metamorphic and associated rocks in the Central South Carpathians. An. Inst. Geol. Geof. LXI, 31–38.

Harrison, T.M., Watson, E.B., 1984. The behavior of apatite during crustal anatexis: equilibrium and kinetic considerations. Geochim. Cosmochim. Acta 48, 1467–1477.

Hofmann, A.W., 1980. Diffusion in natural silicate melts: a critical review. In: Hargraves, R.B. (Ed.), Physics of Magmatic Processes, Princeton University Press, Princeton, pp. 385–417.

Kress, V., Carmichael, I., 1991. The compressibility of silicate liquids containing Fe$_2$O$_3$ and the effect of composition, temperature, oxygen fugacity and pressure on their redox states. Contrib. Mineral. Petrol. 108, 82–92.

Le Maitre, R.W., 1989. A Classification of Igneous Rocks and Glossary of Terms. Blackwell, Oxford.

Lesher, C.E., 1990. Decoupling of chemical and isotopic exchange during magma mixing. Nature 344, 235–237.

Liégeois, J.-P., Black, R., 1987. Alkaline magmatism subsequent to collision in the Pan-African belt of the Adrar des Iforas. In: Fitton, J.G., Upton, B.G.J. (Eds.), Alkaline Igneous Rocks, The Geological Society. Blackwell, pp. 381–401.

Liégeois, J.-P., Black, R., Navez, J., Latouche, L., 1994. Early and late Pan-African orogenies in the Aïr assembly terranes (Tuareg shield, Niger). Precambr. Res. 67, 59–88.

Liégeois, J.-P., Berza, T., Tatu, M., Duchesne, J.C., 1996. The Neoproterozoic Pan-African basement from the Alpine lower Danubian nappe system (South Carpathians, Romania). Precambrian Res. 80, 281–301.

McBirney, A.R., Baker, B.H., Nilson, R.H., 1985. Liquid fractionation: Part I. Basic principles and experimental simulations. J. Volc. Geotherm. Res. 24, 1–24.

Nelson, B.K., DePaolo, D.J., 1985. Rapid production of continental crust 1.7 to 1.9 b.y. ago: Nd isotopic evidence from the basement of the North American mid-continent. Geol. Soc. Am. Bull. 96, 746–754.

Nevez, S.P., Vauchez, A., 1995. Successive mixing and mingling

of magmas in a plutonic complex of Northeast Brazil. Lithos 34, 275–299.

Nielsen, R.L., 1988. A model for the simulation of combined major and trace element liquid line of descent. Geochim. Cosmochim. Acta 52, 27–38.

Pitcher, W.S., 1993. The Nature and Origin of Granite. Blackie Academic and Professional, London.

Provost, A., Allègre, C.J., 1979. Process identification and search for optimal parameters from major-element data. General presentation with emphasis on the fractional crystallization process. Geochim. Cosmochim. Acta 43, 77–107.

Rickwood, P.C., 1989. Boundary lines within petrologic diagrams which use oxides of major and minor elements. Lithos 22, 247–264.

Roberts, M.P., Clemens, J.D., 1995. Feasibility of AFC models for the petrogenesis of calc-alkaline magma series. Contrib. Mineral. Petrol. 121, 139–147.

Roberts, M.P., Clemens, J.D., 1997. Correction to Roberts and Clemens (1995) 'Feasibility of AFC models for the petrogenesis of calc-alkaline magma series'. Contrib. Mineral. Petrol. 128, 97–99.

Schmidt, M.W., 1996. Experimental constraints on recycling of potassium from subducted oceanic crust. Science 272, 1927–1930.

Spear, F.S., 1993. Metamorphic Phase Equilibria and Pressure–Temperature–Time Paths. Mineral. Soc. Amer., Washington, DC, 799 p.

Steiger, R.H., Jäger, E., 1977. Subcommission on geochronology: convention on the use of decay constant in geo- and cosmochronology. Earth Planet. Sci. Lett. 36, 359–362.

Sylvester, P.J., 1989. Post-collisional alkaline granites. J. Geol. 97, 261–280.

Tatu, M., Berza, T., 1994. Rapakivi structure in the Tismana granitoid (abstract). 16th Gen. Meet. IMA, Pisa, 405.

Turner, S., Arnaud, N., Liu, J., Rogers, N., Hawkesworth, C., Harris, N., Kelley, S., Van Calsteren, P., Deng, W., 1996. Post-collision, shoshonitic volcanism on the Tibetan plateau: implications for convective thinning of the lithosphere and the source of ocean island basalts. J. Petrol. 37, 45–71.

Vander Auwera, J., Bologne, G., Roelandts, I., Duchesne, J.C., 1999. Inductively coupled plasma-mass spectrometry (ICP-MS) analysis of silicate rocks and minerals. Geologica Belgica 1, 1–10.

Vander Auwera, J., Longhi, J., Duchesne, J.C., 1998. A liquid line of descent of the jotunite (hypersthene monzodiorite) suite. J. Petrol. 39, 439–468.

van Marcke de Lummen, G., Vander Auwera, J., 1990. Petrogenesis of the Traversella diorite (Piemonte, Italy): a major-and trace-element and isotopic (O, Sr) model. Lithos 24, 121–136.

Vernon, R.H., 1986. K-feldspar megacrysts in granites—phenocrysts not porphyroblasts. Earth-Sci. Rev. 23, 1–63.

Warner, M., Morgan, J., Barton, P., Morgan, P., Price, C., Jones, K., 1996. Seismic reflections from the mantle represent relict subduction zones within the continental lithosphere. Geology 24, 39–42.

Watson, E.B., Green, T.H., 1981. Apatite/liquid partition coefficients for the rare earth elements and strontium. Earth Planet. Sci. Lett. 56, 405–421.

Watson, E.B., Harrison, T.M., 1983. Zircon saturation revisited: temperature and compositional effects in a variety of crustal magma types. Earth Planet. Sci. Lett. 64, 295–304.

Whalen, J.B., Currie, K.L., Chappell, B.W., 1987. A-type granites: geochemical characteristics, discrimination and petrogenesis. Contrib. Mineral. Petrol. 95, 407–419.

Whittaker, E.J.W., Muntus, R., 1970. Ionic radii for use in geochemistry. Geochim. Cosmochim. Acta 34, 945–956.

Wilson, J.R, Robins, B., Nielsen, F., Duchesne, J.C., Vander Auwera, J., 1996. The Bjerkreim–Sokndal layered intrusion, Southwest Norway. In: Cawthorn, R.G. (Ed.), Layering in Igneous Complexes. Elsevier, Amsterdam, pp. 231–256.

Zhang, M., Suddaby, P., Thompson, R.N., Thirlwall, M.F., Menzies, M.A., 1995. Potassic volcanic rocks in NE China: geochemical constraints on mantle source and magma genesis. J. Petrol. 36, 1275–1303.